

Hydrothermal Sol-gel TiO₂ Nanoparticles fixed to Clay and its Photocatalytic Application for the Degradation of Methyl Orange

Aliou Pohan^{1,*}, Hervé Goure-Doubi¹, Amadou Kouyate², Muhammad Nasir³, Maria Visa⁴ and Lassiné Ouattara⁵

¹ Training and Research Unit of Biological Sciences, Péléforo Gon Coulibaly University of Korhogo, BP 1328 Korhogo, Ivory Coast

² Jean Lorougnon Guédé University, BP 150 Daloa, Ivory Coast

³ Interdisciplinary Research Centre in Biomedical Materials, COMSAT Institute of Information Technology (CIIT), Defence Road, Off Raiwind Road, Lahore 54000, Pakistan

⁴ Transilvania University of Brasov, RTD Dept. Renewable Energy Systems and Recycling, Romania, Eroilor 29, 500036 Brasov, Romania

⁵ Laboratory of Physical Chemistry, UFR SSMT, Félix Houphouët-Boigny University of Cocody, Abidjan, 22 BP 582 Abidjan 22, Ivory Coast

Abstract: In this paper, Clay-TiO₂ nanomaterials were synthesized via hydrothermal sol-gel method using Ivorian clays and titanium tetra-isopropoxide as precursors. The synthesized composite was characterized through XRD, SEM/EDX, FTIR and BET surface measurements. The photocatalytic activity of composite towards the degradation of methyl orange (MO), a model pollutant, has been investigated under UV and simulated solar radiation. Comparative experiments done in a solution with and without H₂O₂ indicate an increase in efficiency for methyl orange removal from the polluted water in the presence of H₂O₂. The optimized parameters (contact time, amount of nanocomposite and amount of Fe²⁺/H₂O₂) allowed to reach removal efficiency up to 60 % of MO. Immobilization of TiO₂ on clay facilitate repeated using of nanomaterials, two times.

Keywords: Titanium dioxide; clay; nanocomposite; photocatalysis; methyl orange degradation; Hydrothermal sol-gel.

1. Introduction

Textile and other industrial dyes cause an increased environmental threat to the ecosystem and its preservation. These dyes mainly include azo groups (N=N) combined with benzene or naphthalene rings^{1,2}. More than 10% of the total dyestuff is used for the dyeing of cotton products, whereas up to 30% of the used azo dyes discarded into the environment after they have been utilized in dyeing^{3,4,5}. For this purpose, dye removal or degradation from wastewater has been extensively studied to reduce its adverse impact on the environment. The conventional methods of removing these pollutants are chemical coagulation⁶, electro-flocculation and biological treatment⁷, photocatalysis⁸, Fenton⁹, nanofiltration membranes^{10,11} and adsorption¹².

Photocatalysis is being focused largely from the last three decades and is expected to be a promising alternative to the reduction of environmental pollutants¹³. This technique is defined as a process

that occur at normal temperature conditions involving the generation of highly reactive species (the hydroxyl radical) in an amount sufficient to be effective in water purification processes. The generation of free radicals is initiated by the interaction of photons with the molecules or chemical species present in solution or with a catalyst⁸. High photocatalytic properties of certain semiconducting materials have been used to convert solar energy into chemical energy to remove pollutants and bacteria¹⁴ on wall surfaces, in air and water¹⁵. Among different types of photocatalysts used for degradation of pollutants¹⁶, titanium dioxide (TiO₂) is usually chosen due to its strong oxidizing and antibacterial abilities¹⁷, its superhydrophilicity¹⁸, chemical stability, long durability, nontoxicity, low cost and easy availability. Although TiO₂ was excellent photocatalyst, his practical application is hindered by a lack of visible-light absorption and the low quantum efficiency¹⁹. In addition, his recycling for repeated use is difficult^{20,21}. A straightforward method to solve the problem is to immobilizing TiO₂.

*Corresponding author: Aliou Pohan

Email address: pohan.aliou@gmail.com

DOI: <http://dx.doi.org/10.13171/mjc92190918430ap>

Received August 27, 2019

Accepted September 20, 2019

Published September 18, 2019

As a response, several workers have coated photocatalysts (TiO_2) onto a variety of surfaces, such as glass silica gel, metal, ceramics, polymer, activated carbon^{22,23}.

In this study, the application of TiO_2 immobilized on clay from Côte d'Ivoire for wastewater treatment is reported. An aqueous solution containing methyl orange (MO) was selected as a model compound to simulate the industrial wastewater. The obtained results suggest that TiO_2 nanoparticles immobilized on Clay can be used as a photocatalytic agent for the degradation of organic pollutants in the environment, especially in aqueous media. This work is a novelty in order to contribute to the valorisation of clays, especially those of Côte d'Ivoire.

2. Experimental

2.1. Raw material

The clay material used in this work was collected from the Hambol region (North of Côte d'Ivoire), precisely in the town of Katiola. The clay was named according to their color in French (Rouge (R)). These clays are extracted from quarries located around the geographical coordinates: $08^{\circ}09.030'$ North, $005^{\circ}05.850'$ West and altitude 996 m extend over about 10 Km^2 at a depth of 1.5m.

2.2. Reagents

Titanium tetra-isopropoxide ($\geq 99\%$), sodium hydroxide (NaOH , $\geq 99\%$) are from Fulka, iron salt ($\text{FeSO}_4 \cdot 7\text{H}_2\text{O}$ (98.99% purity) and H_2O_2 (30%) are provided by ScharlauChemia S.A, and methyl-orange (E. Merck 99.98% purity). All these reagents were analytic grades and employed without further purification. Distilled water was used throughout all our experiments.

2.3. Synthesis of TiO_2 powder by sol-gel technique

The TiO_2 sol was synthesized by acid catalyzed sol-gel formation method using 60 mL of 1 M HNO_3 and 15 mL of titanium tetra-isopropoxide following by the hydrolysis reaction²⁴. Briefly, titanium tetra-isopropoxide was added gradually to the aqueous solution of HNO_3 solution under continuous stirring for 3 hours to produce a transparent sol. Subsequently, the pH of the colloid solution was adjusted to 3 with the addition of 1 M NaOH , which results in a turbid colloid. The mixed suspension was then stirred for another 2 hours at room temperature, followed by filtration (Millipore $0.45 \mu\text{m}$) and repeatedly washing with de-ionized water until the pH of the supernatant was about 6. The resulting TiO_2 was dried in a furnace for 1 hour at 100°C and finally, the powder was annealed at 500°C for 3 hours.

2.4. Preparation of Clay- TiO_2 nanomaterials

For repeated use of nanocomposite, TiO_2 nanoparticles were immobilized on clay. Clay- TiO_2 was synthesized by simple mixing of TiO_2 sol obtained by the process described above and clay previously washed and activated^{25,26} noted RW. The

mixture is realized before the final calcination at 500°C for 3 hours, according to mass ratio 1:1. The nanocomposite obtained has been noted R- TiO_2 .

2.4. Characterization of the material substrate

2.4.1. X-ray diffraction

X-ray diffraction (XRD) spectra were obtained using a Bruker multifunctional D8 ADVANCE model diffractometer. XRD experiments were achieved on powdered samples in the step-scan mode in the range $2^{\circ} \leq 2\theta \leq 60^{\circ}$ with a step size of 0.01° (2θ) and a counting time of 0.25s. Phases identification was performed by comparing the X-ray diffraction patterns with the International Center for Diffraction Data (ICDD) using the EVA (Bruker AXS) software.

2.4.2 Specific surface area measurements

The Brunauer Emmett and Teller (BET) method²⁷ was used to determine the specific surface area of the samples, using a TriStar II equipment from Micromeritics. Measurements were carried out after a 16 h degassing step at 200°C .

2.4.3. Scanning Electron Microscopy (SEM)

The microstructural observation of the samples was done using a Scanning Electron Microscopy of the "FEI, Quanta FEG 450, Environmental" type. SEM images were performed on powdered samples. Prior to their observation, a small amount of powder from each sample was suspended in distilled water. After stirring with ultrasound for 5 minutes, a drop of each suspension was placed on a sample holder and then dried.

2.4.4. FTIR analysis

Structural characterization of prepared nanocomposites was analyzed by using Fourier transform infrared (FTIR) spectroscopy, coupled with smart ATR accessory and photoacoustic sampling cells. Spectra were recorded within the wavelength range of $4000\text{-}400 \text{ cm}^{-1}$, with average 256 numbers of scans at 8 cm^{-1} resolution on a Thermo- Nicolet 6700P FTIR Spectrometer (USA)

2.5. Photocatalysis experiments

Batch photocatalysis experiments were done at room temperature, under stirring (using magnetic stirrer VELP Scientifica ARE-6, at 100 rpm). In all the experiments, a constant ratio substrate mass: solution volume was set at 0.1 g (TiO_2 sol mixing to clay: R- TiO_2):50 mL. The adsorption mechanisms and the kinetic data were evaluated on two types of suspensions:

(1) R- TiO_2 + MO ($C_{\text{MO}} = 0.0125 \text{ mM}$); this concentration was chosen as it is a usual upper limit of the industrial wastewaters subject of investigations²⁸.

(2) R- TiO_2 + MO ($C_{\text{MO}} = 0.0125 \text{ mM}$) + Fenton system ($\text{FeSO}_4 + \text{H}_2\text{O}_2$). The volume of H_2O_2 was kept constant at $10 \mu\text{L}$ and Fe^{2+} $20 \mu\text{L}$.

In the kinetic studies, aliquots were taken at pre-set moments (up to 360 min), when stirring was briefly interrupted and, after filtration on a 0.45 mm filter, the supernatant was analysed. Preliminary experiments proved dye losses (adsorption on the beaker walls and the filtering paper) were negligible. The photocatalysis experiments have been repeated two times by reusing the photocatalyst, previously washed (in 0.1 N NH_3) and dried.

Photodegradation studies were done on R-TiO₂ suspensions with an identical overall concentration of the dispersed phase, with/without Fenton reactive and hydrogen peroxide (30%) under UV irradiation using quartz beakers. The homemade reactor is equipped with three F18 W/T8 blacklight tubes (Philips), emitting UV light, typically 340–400 nm, with λ_{max} (emission) = 365 nm²⁹. The mean value of the radiation flux intensity, reaching the middle of the reacting suspension was 3 Lx (Mavolux5032B/USM), and the irradiance is 846 W m⁻². During the investigations the radiation flux intensity was in the range of 0.7–1.6 Lx with average irradiation of 215 W m⁻².

2.6. Pollutants analysis

The MO was analysed by UV–vis spectrophotometry (Perkin Elmer Lambda 25), on the calibration curve registered at $\lambda = 460$ nm. The amount of pollutants uptake by adsorbents (adsorption capacity), q_t , the removal efficiency, η , percentage were calculated using the following Eqs. (1) and (2).

$$\eta = \frac{c_0 - c_t}{c_0} \times 100 \quad (1)$$

$$q_t = \frac{c_0 - c_t}{m} \times V \quad (2)$$

where c_0 represents the initial concentration of the pollutants; c_t represents the concentration of the pollutants at the time t ; V the solution volume (L) and m , the amount of substrate (g).

3. Results and Discussion

3.1. Substrate characterization

The structure of the synthesized composite was investigated using X-ray diffraction. The diffraction patterns are shown in Figure 1 A and B for RW and R-TiO₂, respectively. For the RW (Figure 1A), the X-ray spectrum shows two peaks located at 10.23° and 24.95°, which are characteristic of kaolinite^{30–32}. Also, high and low intensity of quartz peaks located at 20° 21°, 39.2°, 40° and 42.3° are observed³³. Quartz is a commonly found mineral in the earth's continental crust, which satisfy the appearance of these peaks. Further, the presence of iron is confirmed by goethite peaks at 34.1° and 36°. The presence of iron ions could explain the red color of the clays used. The peaks of illite are observed at 9°, 18° and 46°³⁴. After the addition of TiO₂, the anatase diffraction peaks were detected in the X-ray spectrum of R-TiO₂ (Figure 1B).

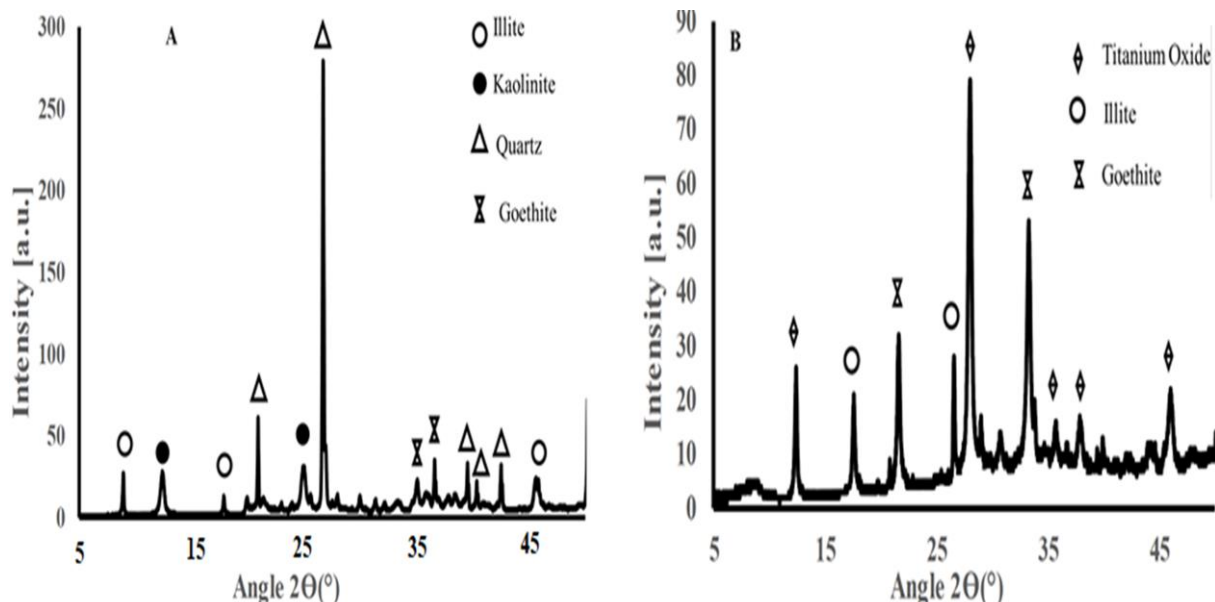


Figure 1. XRD diagrams ((A): RW and (B): R-TiO₂)

The sharpest peak of anatase appeared at 12.0°, and other peaks are detected at 36.0°, 38.1° and 46.0°. Thus, during the synthesis of TiO₂ by the sol-gel process, the calcination at 500 °C produce mainly the anatase phase of TiO₂. The specific surface area of

RW and R-TiO₂ was obtained as 11.48 and 19.12 m². g⁻¹ respectively as measured through BET pore size and surface area analyzer. These values of the specific surface area are in concordance with the values found in literature^{35,36}. In the presence of TiO₂, the surface area

increases (from 11.48 to 19.12 m² g⁻¹). This result was also observed by Soro et al.³⁷ during their works.

To better access, the structure of the synthesized compounds, SEM and FTIR techniques were done. The results are shown in Figure 2 and Figure 3, respectively. Figure 2A show platelets of kaolinite

and grains of quartz. These results are in correlation with X-Ray diffraction analysis. In Figure 2B, we observe a modification of surface morphology of clay. The micrograph of R-TiO₂ shows aggregates formation.

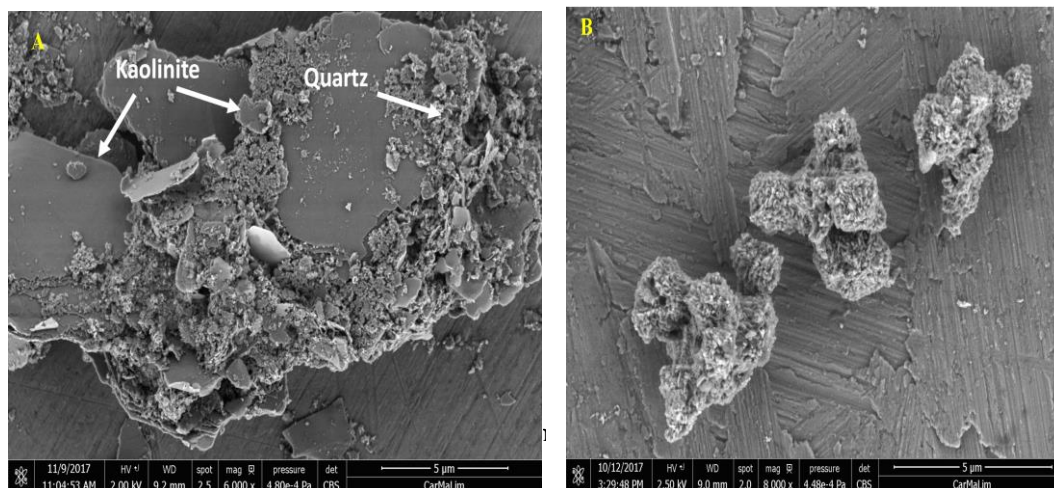


Figure 2. SEM micrograph of RW(A) and R-TiO₂ (B)

On Figure 3, the spectra show peaks around 3500 cm⁻¹ arises due to the presence of OH stretching vibration in the Titania samples as Ti-OH. These peaks around 1000 cm⁻¹ could be attributed to the

added functional groups related to oxygen in Titania. The peaks observed around 2360 cm⁻¹ represent CO₂ adsorbed²⁵.

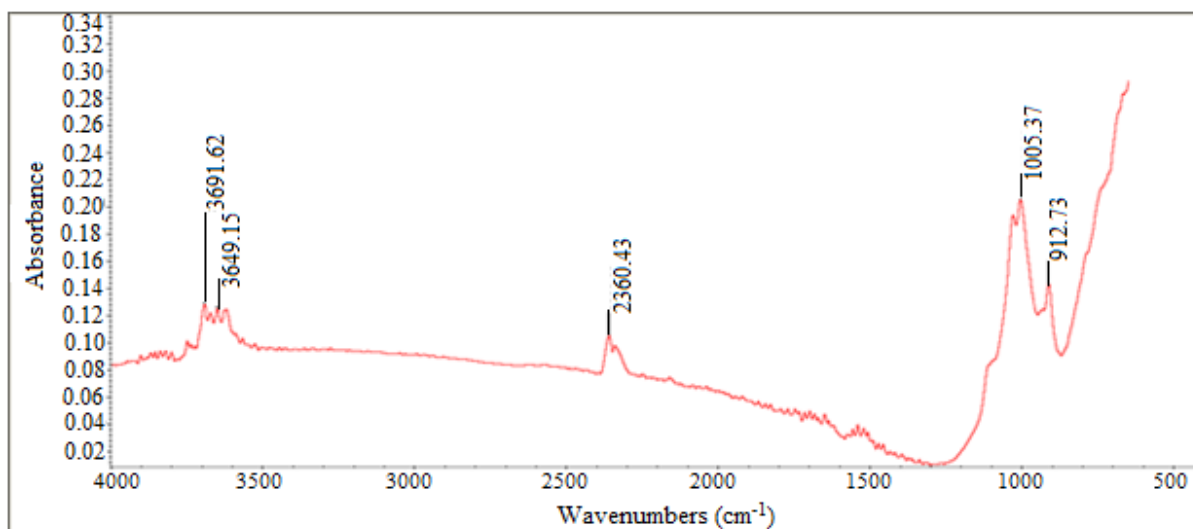


Figure 3. FTIR of R-TiO₂

3.2. Photocatalytic activity of R-TiO₂

The photocatalytic activity of R-TiO₂ was investigated by monitoring the decrease in the concentration 50 ml of 0.0125 mM solution of Methyl Orange (MO) in the presence of the 0.1 g of prepared photocatalyst under UV irradiation at room temperature. All values (equilibrium time and MO concentration) were chosen in function of our previous work²⁸. Precisely, the process consists of two parts: dark adsorption and photodegradation. In the dark adsorption process (30 min), the

concentration of MO in the solution decreases slowly. The lower efficiencies are the result of the molecular structure of MO, Figure 4. MO is an azo (-N=N-) group compound with a diethylamine group side substituent on one of the aromatic rings. When ionized in water, a negatively charged chromophore is produced, so that MO is also known as an anionic dye or acidic dye. After the 30min dark adsorption, η is 5.45 %.

The photocatalytic properties of the synthesized material were evaluated using MO as a pollutant in

aqueous media. Figure 5 shows the time-dependent UV/Vis absorption measurement of methyl orange degradation.

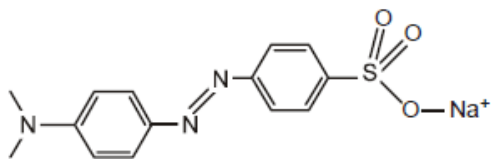


Figure 4. The structure of Methyl orange³⁸

At $t = 0$ min, the curve is associated with the absorption spectrum of methyl orange solution

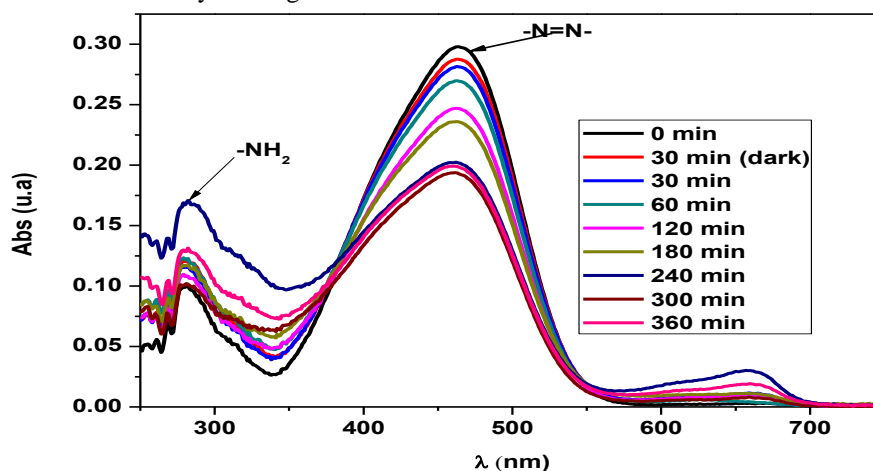


Figure 5. Time-dependent UV/Vis absorption measurement of methyl orange photodegradation.

In the photodegradation process, the concentration of MO decreases by 9.54% of the initial value within a short period of 60 min, indicating the good photocatalytic activity of the R-TiO₂. In this work, the TiO₂ nanoparticles are uniformly dispersed onto the washed clay (Figure 2) in the as-prepared composite catalyst, leading to high specific surface area and increased reaction sites. Therefore, both the adsorption and photochemical reactions are accelerated in the composite catalyst (R-TiO₂), which is responsible for its good photocatalytic activity in the degradation of MO.

The degradation of MO by photocatalysis and photo-Fenton are presented in Figure 6. As can be seen, MO removal efficiency increase using the Fenton system (H₂O₂/Fe²⁺/Fe³⁺). After 60 min, 15.02 % of MO was removed and removal efficiency up to 60 % after 360 min. The mixture of H₂O₂ and Fe²⁺ in medium leads to the promotion of hydroxyl radicals which efficiently oxidize the organic pollutants⁴⁰. The similar results have been observed by M. Visa et al. with FA: TiO₂ photocatalysts²⁶.

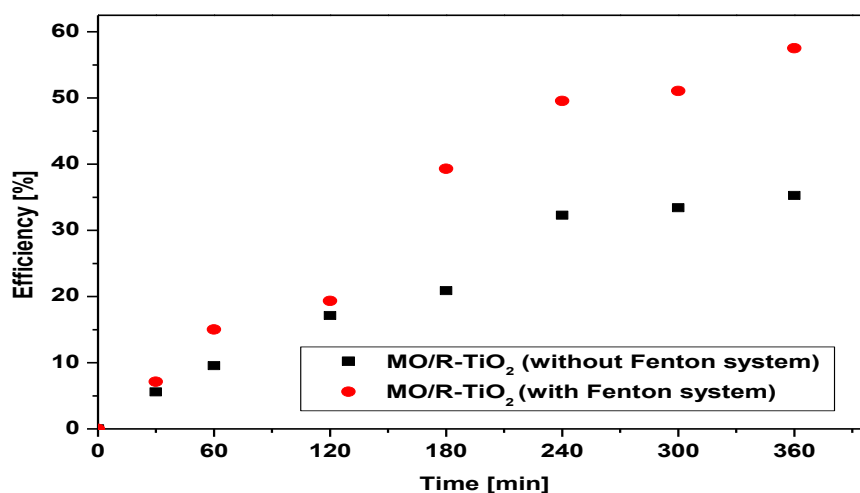
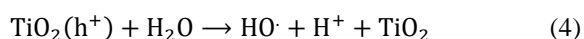
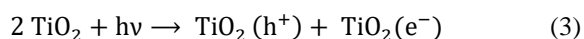


Figure 6. Methyl-orange removal efficiency on R-TiO₂ with and without Fenton system.

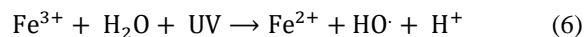
The combination of hydrogen peroxide and UV radiation with a Fe^{2+} ion produces more hydroxyl radicals, and in turn, it increases the rate of degradation of organic pollutants. Fenton reaction accumulates Fe^{3+} ions in the system, and the reaction does not proceed, once all Fe^{2+} ions are consumed. The photochemical regeneration of ferrous ions by photo-reduction of ferric ions occurs in the photo-Fenton reaction. The newly generated ferrous ions react again with H_2O_2 generating hydroxyl radical and ferric ion, and in this way, the cycle continues⁴¹.

3.3. Degradation mechanism

On the new composite (R-TiO₂), TiO₂ is activated when irradiated with energy higher than the bandgap value ($E_g = 3.1$ eV, corresponding to $\lambda = 399.9$ nm). Under irradiation, electron-hole pairs are photo-generated (Eq.3); the holes will most likely react with water to form active oxidant species HO[•](Eq.4) that may degrade the organic dye (MO)²⁸.



In the photo-Fenton system, supplementary amounts of HO[•] are produced from the fast hydrogen peroxide decomposition:



Thus, the mechanism for methyl orange degradation using R-TiO₂ can be proposed as below: When the photocatalyst is introduced, the methyl orange molecule was first adsorbed on the surface of the nanocomposite, then the TiO₂ present on the surface reacted with the $-\text{N}=\text{N}-$ double bond and broke it to single phenyl ring compounds with amine group as possible products. In addition, HO[•] products by photo-Fenton acts directly with MO in the medium.

3.4. Kinetic study

In the photodegradation process, the kinetics of the photocatalytic degradation is described using the pseudo-first-order model (Eq.8), and the results are displayed in Figure 7.

$$\ln\left(\frac{C_t}{C_0}\right) = -k_a t \quad (8)$$

where C_0 is the initial concentration of MO; C_t is the concentration of MO at time t , and k_a (min^{-1}) is the apparent pseudo-first-order decay rate constant which can be obtained by plotting $\ln(C_t/C_0)$ vs. t as shown in Figure 6⁴². The values of rate constants confirm that HO[•] in solution increases the kinetic of MO degradation on R-TiO₂.

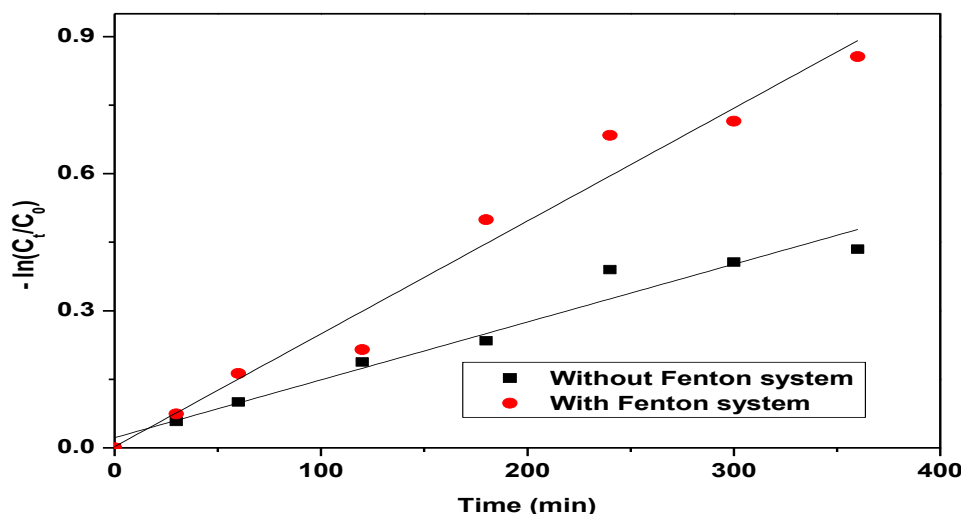


Figure 7. Kinetic of photodegradation of MO on R-TiO₂

4. Conclusion

TiO₂ nanoparticles were successfully prepared by sol-gel method and immobilized on clay via hydrothermal method. This immobilization of TiO₂ on clay facilitate repeated using of nanomaterials. From the R-TiO₂ samples, only anatase phase was confirmed from the XRD results. The SEM and FTIR analysis results confirmed the modification of morphology surface of clay by TiO₂ incorporation. In this work, the presence of TiO₂ on the clay raise weakly its surface specific area from 11.48 to 19.12 $\text{m}^2 \text{g}^{-1}$. The photocatalytic degradation of mono azo dye MO was investigated using R-TiO₂ nanocomposite in aqueous solution

under sunlight. This study demonstrated the effectiveness of nanomaterials in methyl orange degradation. The presence of the anatase phase of TiO₂ nanoparticles should be responsible for the best catalytic activity of R-TiO₂. However, the kinetics of degradation of MO increases in the presence of HO[•] in the media. These results suggest that R-TiO₂ can be a powerful tool for organic pollutants remover in aqueous media.

5. Acknowledgments

This work is supported by Agence Universitaire de la Francophonie (Eugen Ionescu scholarship)

References

- 1- Atcharyawut S, Phattaranawik J, Leiknes T, et al. Separation and Purification Technology, **2009**, 66(1), 153-158.
- 2- L. Jian-hua, W. Hai-jun, Journal of Chongqing University (English Edition), **2009**, Vol. 8, No. 3
- 3- J. Easton, Colour in Dye House Effluent, Alden Press, Oxford, **1995**, 9-21.
- 4- K. Selvam, K. Swaminathan, C. Keo-Sang, World J Microbiol Biotechnol., **2003**, 19, 591-593.
- 5- R.J. Maguire, Occurrence and persistence of dyes in a Canadian river, Water Sci Technol., **1992**, 25, 265.
- 6- L. Shamaei, B. Khorshidi, B. Perdicakis, M. Sadrzadeh, Treatment of oil sands produced water using combined electrocoagulation and chemical coagulation techniques, Science of the Total Environment, **2018**, 645, 560-572.
- 7- A.H. Konsowa, Decolorization of wastewater containing direct dye by ozonation in a batch bubble column reactor, Desalination, **2003**, 158, 233-240.
- 8- H. Lei, H. Zhang, Y. Zou, X. Dong, Y. Jia, F. Wang, Synergetic photocatalysis/piezocatalysis of bismuth oxybromide for degradation of organic pollutants, Journal of Alloys and Compounds, **2019**, 809, 151840.
- 9- J. N. Göde, D. H. Souza, V. Trevisan, E. Skoronski. Application of the Fenton and Fenton-like processes in the landfill leachate tertiary treatment, Journal of Environmental Chemical Engineering, **2019**, 7, 103352
- 10- Y. Li, Y. J. Zhao, H. Wang, M. Wang, the application of nanofiltration membrane for recovering lithium from Salt Lake brine, Desalination, **2019**, 468, 114081.
- 11- H.F. Xiao, C.H. Chu, W.T. Xu, B.Z. Chen, X.H. Ju, W. Xing, S.P. Sun, Amphibian-inspired amino acid ionic liquid functionalized nanofiltration membranes with high water permeability and ion selectivity for pigment wastewater treatment, Journal of Membrane Science, **2019**, 586, 44-52.
- 12- C. Yao, T. Chen, An improved regression method for kinetics of adsorption from aqueous solutions, Journal of Water Process Engineering, **2019**, 31, 100840.
- 13- M.N. Rashed, A.A. El-Amin, Photocatalytic degradation of methyl orange in aqueous TiO₂ under different solar irradiation sources, Inter J Phy Sci., **2007**, 2, 73-81.
- 14- L. Caballero, K.A. Whitehead, N.S. Allen, J. Verran, Inactivation of Escherichia coli on immobilized TiO₂ using fluorescent light, J. Photochem. Photobiol., **2009**, A 202, 92-98.
- 15- A. Fujishima, K. Hashimoto, T. Watanabe, TiO₂ Photocatalysis: Fundamentals and Applications, BKC, Tokyo, **1999**.
- 16- E.N.S. Pelizzetti (Ed.), Homogeneous and Heterogeneous Photocatalysis, D. Reidel Publishing Company, Dordrecht, **1986**.
- 17- Y. Nosaka, T. Daimon, A.Y. Nosaka, Y. Murakami, Singlet oxygen formation in photocatalytic TiO₂ aqueous suspension, **2004**, PCCP 6, 2917-2918.
- 18- R. Wang, K. Hashimoto, A. Fujishima, M. Chikuni, E. Kojima, A. Kitamura, M. Shimohigoshi, T. Watanabe, Light-induced amphiphilic surfaces, Nature, **1997**, 388, 431-432.
- 19- S. Sarina, E.R. Waclawik, H. Zhu, Photocatalysis on supported gold and silver nanoparticles under ultraviolet and visible light irradiation, Green Chem., **2013**, 15, 1814-1833.
- 20- J.A. Byrne, B.R. Eggins, N.M.D. Brown, B. McKinney, M. Rouse, Immobilisation of TiO₂ powder for the treatment of polluted water, Appl. Catal., **1998**, B 17, 25-36.
- 21- N.M. Mahmoodia, M. Arami, N.M. Mahmoodi, M. Arami, Bulk phase degradation of Acid Red 14 by nanophotocatalysis using immobilized titanium (IV) oxide nanoparticles, J. Photochem. Photobiol., **2006**, A 182, 60-66.
- 22- I. Turkevych, Y. Pihosh, M. Goto, A. Kasahara, M. Tosa, S. Kato, K. Takehana, T. Takamasu, G. Kido, N. Koguchi, Photocatalytic properties of titanium dioxide sputtered on a nanostructured substrate, Thin Solid Films, **2008**, 516, 2387-2391.
- 23- M. Huang, C. Xu, Z. Wu, Y. Huang, J. Lin, J. Wu, Photocatalytic Discolorization of Methyl Orange Solution by Pt Modified TiO₂ Loaded on Natural Zeolite, Dyes Pigments, **2008**, 77, 327-334.
- 24- L. Andronic, A. Duta, Photodegradation process in two dyes systems -simultaneous analysis by first-order spectra derivative method, Chem. Eng. J., **2012**, 198-199, 468-475.
- 25- P.L.A. Guillaume, A.M. Chelaru, M. Visa, O. Lassiné, Titanium Oxide- Clay as Adsorbent and Photocatalysts for Wastewater Treatment. J Membra Sci Technol, **2017**, 176. Doi: 10.4172/2155-9589.1000176
- 26- M. Visa, A. Duta, enhanced heavy metals adsorption on dye - modified fly ash, J. Environ. Eng. Manage, **2009**, 8, 803-808.
- 27- S. Brunauer, P. Emmett, E. Teller, Adsorption of Gases in Multimolecular Layers, J. Am. Chem. Soc., **1938**, 60, 309-319.
- 28- M. Visa, A. Duta, Methyl-orange and cadmium simultaneous removal using fly ash and photo-Fenton systems Journal of Hazardous Materials, **2013**, 244-245, 773-779.
- 29- A. Khorsand Zak, W.H.A. Majid, M.E. Abrishami, R. Yousefi, R. Parvizi, Synthesis, magnetic properties and X-ray analysis of Zn_{0.97}X_{0.03}O nanoparticles (X = Mn Ni, and Co) using Scherer and size-strain plot methods, Solid State Sci., **2012**, 14 (4), 488-494.
- 30- J.J. Tunney, C. Detellier, Aluminosilicate Nanocomposite Materials. Poly (ethylene

- glycol)-Kaolinite Intercalates, *Chem. Mater.*, **1996**, 8, 927-935.
- 31- A.M.S., Al-Shenti, *Geology of The Arabian Shield*, Copy 2. Jeddah, **2003**, p. 204.
- 32- Q. Mohsen, A. El-maghraby, Characterization and assessment of Saudi clays raw material at a different area, *Arabian Journal of Chemistry*, **2010**, 3, 271-277.
- 33- H. Goure-Doubi, C. Martias, G. L. Lecomte-Nana, B. Nait-Ali, A. Smith, E. Thune, N. Villandier, V. Gloaguen, M. Soubrand, L. K. Konan, Interfacial reactions between humic-like substances and lateritic clay: Application to the preparation of “geomimetic” materials *Journal of Colloid and Interface Science*, **2014**, 434, 208-217.
- 34- H.G. Doubi, A.N. Kouamé, Konan, L.K., Tognonvi, M. and Oyetola, S. Thermal Conductivity of Compressed Earth Bricks Strengthening by Shea Butter Wastes with Cement. *Materials Sciences and Applications*, **2017**, 8, 848-858.
- 35- J. Guyot, Mesure des surfaces spécifiques des argiles par adsorption. *Ana. Agron.*, **1969**, 20(4), 333-359.
- 36- B. Plešingerová, G. Súčik, M. Fabián, Surface area change of kaolin causing annealing, *Acta Metallurgica Slovaca*, **2011**, Vol. 17, No. 3, 169-176.
- 37- G. Lecomte-Nana, J.P. Bonnet, N. Soro, Influence of iron onto the structural reorganization process during the sintering of kaolins, *J. Eur. Ceram. Soc.*, **2013**, 33, 661-668.
- 38- C.S. Keng, Z. Zainal, A.H. Abdullah, Removal of cationic and anionic dyes by immobilized titanium dioxide loaded activated carbon, *The Malaysian Journal of Analytical Sciences.*, **2008**, vol. 12, no.2, 451-457.
- 39- Y. Sha, I. Mathew, Q. Cui, M. Clay, F. Gao, X. J. Zhang, Z. Gu, Rapid degradation of azo dye methyl orange using hollow cobalt nanoparticles, *Chemosphere*, **2016**, 144, 1530-1535.
- 40- H.J.H. Fenton, Oxidation of tartaric acid in the presence of iron. *Journal of the Chemical Society*, **1894**, Vol. 65, pp. 899-901, ISSN 0368-1769.
- 41- R. Ameta, K. A. Chohadia, A. Jain, & P. B. Punjabi, Fenton and photo-Fenton processes. *Advanced Oxidation Processes for Waste Water Treatment*, **2018**, 49-87.
- 42- H. Shen, C. Duan, J. Guo, N. Zhao, J. Xu, Facile in situ synthesis of silver nanoparticles on boron nitride nanosheets with enhanced catalytic performance. *J. Mater. Chem.*, **2015**, A3, 16663-16669.